Joint short- and long-baseline constraints on light sterile neutrinos

F. Capozzi,[1,2] C. Giunti,[3] M. Laveder,[1,2] and A. Palazzo[4,5]

[1] *Dipartimento di Fisica e Astronomia "Galileo Galilei", Università di Padova, Via F. Marzolo 8, I-35131 Padova, Italy*
[2] *Istituto Nazionale di Fisica Nucleare (INFN), Sezione di Padova, Via F. Marzolo 8, I-35131 Padova, Italy*
[3] *Istituto Nazionale di Fisica Nucleare (INFN), Sezione di Torino, Via P. Giuria 1, I-10125 Torino, Italy*
[4] *Dipartimento Interateneo di Fisica "Michelangelo Merlin," Via Amendola 173, 70126 Bari, Italy*
[5] *Istituto Nazionale di Fisica Nucleare, Sezione di Bari, Via Orabona 4, 70126 Bari, Italy*

Recent studies have evidenced that long-baseline (LBL) experiments are sensitive to the extra CP-phases involved with light sterile neutrinos, whose existence is suggested by several anomalous short-baseline (SBL) results. We show that, within the 3+1 scheme, the combination of the existing SBL data with the LBL results coming from the two currently running experiments NOνA and T2K, enables us to simultaneously constrain two active-sterile mixing angles θ_{14} and θ_{24} and two CP-phases $\delta_{13} \equiv \delta$ and δ_{14}. The two mixing angles are basically determined by the SBL data, while the two CP-phases are identified by the LBL experiments, once the information coming from the SBL setups is taken into account. We also assess the robustness/fragility of the estimates of the standard 3-flavor parameters in the more general 3+1 scheme. To this regard we find that: i) the indication of CP-violation found in the 3-flavor analyses persists also in the 3+1 scheme, with $\delta_{13} \equiv \delta$ having still its best fit value around $-\pi/2$; ii) the 3-flavor weak hint in favor of the normal hierarchy becomes even less significant when sterile neutrinos come into play; iii) the indication of non-maximal θ_{23} (driven by NOνA) appears to be robust in the 3+1 scheme; iv) the preference in favor of one of the two octants of θ_{23} found in the 3-flavor framework (higher octant for inverted mass hierarchy) is completely washed out in the 3+1 scheme.

arXiv:1612.07764v2 [hep-ph] 10 Jan 2017

I. INTRODUCTION

The massive nature of neutrinos and their mixing have been established by a plethora of experiments performed in the last two decades with natural and artificial neutrino sources. The 3-flavor paradigm has been gradually recognized as the sole framework able to account for all the observations performed at baselines longer than ~ 100 meters. In contrast, the same scheme is not able to explain a series of results recorded at shorter distances dubbed as short-baseline (SBL) anomalies. One possible explanation of the SBL anomalies is provided by a flavor oscillation process mediated by new hypothetical light sterile neutrino states.

In the so-called 3+1 scheme, only one new (essentially sterile) mass eigenstate is introduced, with a squared-mass splitting of the order of $\Delta m^2_{\rm SBL} \sim 1\,{\rm eV}^2$ with respect to the three standard neutrinos. In such a scheme the active-sterile admixture is supposed to be small but large enough to explain the anomalies. The 3+1 scheme predicts by construction sizable effects at the short distances, where the oscillating factor $\Delta_{\rm SBL} = \Delta m^2_{\rm SBL} L/4E$ (L being the baseline and E the neutrino energy) is of order one. A rich program of new SBL experiments is underway with the purpose of detecting the smoking gun of active-sterile neutrino oscillations, i.e., the characteristic L/E dependence of the events rate.

After a hypothetical discovery of a sterile neutrino at SBL experiments, the full exploration of the properties of these particles would need other types of experimental setups. In particular, the SBL experiments would not be able to provide any information on the CP-phases involved in the 3+1 scheme. In fact, the manifestation of CP-violation (CPV) is intimately related to the interference of two distinct frequencies. At the SBL setups only one frequency is observable (the new one), while the other two (atmospheric and solar) are undetectable. Therefore, the SBL searches are blind to the CP-phases involved in the 3+1 scheme.[1]

In the standard 3-flavor framework the CPV is encoded by the CP-phase δ which enters the leptonic mixing matrix. The 3-flavor CPV searches are performed at the long-baseline (LBL) experiments, which can observe the $\nu_\mu \to \nu_e$ transition probability in both the neutrino and antineutrino channels. These setups are designed to maximise the amplitude of the interference between the solar and atmospheric oscillations, which embodies a dependency on the CP-phase δ. As a matter of fact, we have already some intriguing indications on δ coming from the partial [1, 2] (including only LBL data) and global [3–6] analyses, which all point towards nearly maximal CPV with $\delta \sim -\pi/2$. This trend has been recently corroborated by the latest data released by NOνA [7] and T2K [8] at the Neutrino and ICHEP 2016 conferences.

As first evidenced in Ref. [1], in the presence of light sterile neutrinos, the $\nu_\mu \to \nu_e$ transition probability probed at the LBL facilities acquires a new interference term, arising from the interference between the atmo-

[1] In the $3 + N_s$ schemes with $N_s > 1$, CPV could be observed at SBL experiments. However, these setups can probe only a limited number of all the CP phases involved in the model. In contrast, LBL experiments have access to all such phases. For example, in the 3+2 scheme, the SBL experiments are sensitive only to one CP-phase over a total of five CP-phases.

spheric frequency and the new large frequency related to the sterile state. Although the fast oscillations driven by the new frequency are completely averaged out by the finite energy resolution of the detector, nonetheless, they can leave their footprints in the transition probability. This renders the LBL experiments sensitive also to the extra CP-phases involved in the 3+1 scheme. The recent 4-flavor analyses [1, 2] of the data from NOνA and T2K have clearly shown that these two experiments are already sensitive to one of the new CP-phases provided that the active-sterile mixing angles are fixed at their best fit values determined by the SBL 3+1 fits [9–12]. In addition, the prospective study performed in [13] has shown that the sensitivity to the extra CP-phases is expected to improve when NOνA and T2K will reach their full exposures, and will further increase in the next-generation experiment DUNE [14].

In this work, we stick to the real data and take a step forward with respect to the existing works. Instead of fixing the active-sterile mixing angles at their best fit values, we here incorporate a full analysis of all the existing SBL data in combination with the LBL results. In this way we are able to simultaneously constrain the two active-sterile mixing angles θ_{14} and θ_{24} and the two CP-phases $\delta_{13} \equiv \delta$ and δ_{14}. The estimates of the two new mixing angles will be basically determined by the SBL data, while those of the two CP-phases will derive from the LBL experiments, once the information from the SBL setups is considered. In this work, we also assess the robustness/fragility of the estimates of the standard 3-flavor parameters in the more general 3+1 scheme, paying particular attention to the most important properties currently under scrutiny: the mass hierarchy, the CP phase δ, and the atmospheric mixing angle θ_{23}.

The rest of the paper is organized as follows. In Sec. II we briefly introduce the theoretical 3+1 framework. In Sec. III we recall the basic features of the flavor oscillations at short baselines. Section IV deals with the 4-flavor transition probability relevant for the LBL setups. In Sec. V we list the data used in the simulations and describe the details of their numerical analysis. In Sec. VI we present and discuss the results of the analysis. Finally, in Sec. VII we draw our conclusions.

II. THEORETICAL FRAMEWORK

In the 3+1 scheme, the flavor $(\nu_e, \nu_\mu, \nu_\tau, \nu_s)$ and mass eigenstates $(\nu_1, \nu_2, \nu_3, \nu_4)$ are related through a 4×4 mixing matrix, which we parametrize as

$$U = \tilde{R}_{34} R_{24} \tilde{R}_{14} R_{23} \tilde{R}_{13} R_{12}\,, \tag{1}$$

where R_{ij} ($\tilde{R}_{ij}$) is a real (complex) 4×4 rotation in the (i,j) plane, which contains the 2×2 matrix

$$R_{ij}^{2\times2} = \begin{pmatrix} c_{ij} & s_{ij} \\ -s_{ij} & c_{ij} \end{pmatrix} \qquad \tilde{R}_{ij}^{2\times2} = \begin{pmatrix} c_{ij} & \tilde{s}_{ij} \\ -\tilde{s}_{ij}^{*} & c_{ij} \end{pmatrix}, \tag{2}$$

in the (i,j) sub-block, where we have introduced the definitions

$$c_{ij} \equiv \cos\theta_{ij} \qquad s_{ij} \equiv \sin\theta_{ij} \qquad \tilde{s}_{ij} \equiv s_{ij} e^{-i\delta_{ij}}. \tag{3}$$

The parameterization in Eq. (1) has the following features: i) When all the three mixing angles involving the fourth state vanish ($\theta_{14} = \theta_{24} = \theta_{34} = 0$) one recovers the 3-flavor matrix in its standard parameterization. ii) For small values of the mixing angles involving the fourth mass eigenstate, it is $|U_{e4}|^2 = s_{14}^2$, $|U_{\mu4}|^2 \simeq s_{24}^2$ and $|U_{\tau4}|^2 \simeq s_{34}^2$, with an immediate physical interpretation of the new mixing angles. iii) With the leftmost positioning of the matrix $\tilde{R}_{34}$, in vacuum, the LBL $\nu_\mu \to \nu_e$ transition probability is independent of θ_{34} and of the associated CP-phase δ_{34}.

III. FLAVOR CONVERSION AT SHORT BASELINES

Short-baseline experiments are sensitive only to the oscillations generated by the new squared-mass difference $\Delta m^2_{\rm SBL} \sim 1\,{\rm eV}^2$, which in the 3+1 framework is $\Delta m^2_{\rm SBL} = \Delta m^2_{41} \simeq \Delta m^2_{42} \simeq \Delta m^2_{43}$, taking into account that the solar squared-mass difference $\Delta m^2_{\rm SOL} = \Delta m^2_{21} \approx 7.4\times10^{-5}\,{\rm eV}^2$ and the atmospheric squared-mass difference $\Delta m^2_{\rm ATM} = |\Delta m^2_{31}| \simeq |\Delta m^2_{32}| \approx 2.5\times10^{-3}\,{\rm eV}^2$ are much smaller (we use the notation $\Delta m^2_{jk} = m^2_j - m^2_k$).

The effective oscillation probabilities of the flavor neutrinos in short-baseline experiments are given by [15]

$$P^{\rm (SBL)}_{\alpha\beta} \simeq \left| \delta_{\alpha\beta} - \sin^2 2\theta_{\alpha\beta} \sin^2\left(\frac{\Delta m^2_{41} L}{4E}\right) \right|, \tag{4}$$

where $\alpha,\beta = e,\mu,\tau,s$, L is the source-detector distance and E is the neutrino energy. The short-baseline oscillation amplitudes depend only on the absolute values of the elements in the fourth column of the mixing matrix:

$$\sin^2 2\theta_{\alpha\beta} = 4|U_{\alpha4}|^2 \left|\delta_{\alpha\beta} - |U_{\beta4}|^2\right|. \tag{5}$$

Hence, the transition probabilities of neutrinos and antineutrinos are equal and it is not possible to measure any CPV effect generated by the complex phases in the mixing matrix in short-baseline experiments.

The short-baseline anomalies in favor of the existence of active-sterile neutrino oscillations are:

1. The LSND observation of an excess of $\bar{\nu}_e$-induced events in a $\bar{\nu}_\mu$ beam [16, 17].

2. The Gallium neutrino anomaly [18–22], consisting in the disappearance of ν_e measured in the Gallium radioactive source experiments GALLEX [23] and SAGE [24].

3. The reactor antineutrino anomaly [25], which is a deficit of the rate of $\bar{\nu}_e$ observed in several reactor

neutrino experiments in comparison with that expected from the calculation of the reactor neutrino fluxes [26, 27].

IV. FLAVOR CONVERSION AT LONG BASELINES

Let us now come to the transition probability relevant for the LBL experiments T2K and NOνA. In Ref. [1], it has been shown that the probability can be written as the sum of three terms

$$P^{4\nu}_{\mu e} \simeq P^{\rm ATM} + P^{\rm INT}_{\rm I} + P^{\rm INT}_{\rm II} \,. \tag{6}$$

The first term represents the positive definite atmospheric transition probability, which can be expressed as

$$P^{\rm ATM} \simeq \, 4 s^2_{23} s^2_{13} \sin^2 \Delta \,, \tag{7}$$

where $\Delta \equiv \Delta m^2_{31} L/4E$ is the atmospheric oscillating frequency. The second term is related to the interference between the oscillations driven by the solar and atmospheric squared-mass splittings. This term, apart from higher order corrections, coincides with the standard interference term, which makes the transition probability sensitive to the CP-phase $\delta \equiv \delta_{13}$. It can be written as

$$P^{\rm INT}_{\rm I} \simeq \, 8 s_{13} s_{12} c_{12} s_{23} c_{23} (\alpha \Delta) \sin \Delta \cos(\Delta + \delta_{13}) \,. \tag{8}$$

The third term is due to 4-flavor effects and is driven by the interference between the atmospheric frequency and the new large frequency introduced by the fourth mass eigenstate. It takes the form

$$P^{\rm INT}_{\rm II} \simeq \, 4 s_{14} s_{24} s_{13} s_{23} \sin \Delta \sin(\Delta + \delta_{13} - \delta_{14}) \,. \tag{9}$$

This term does not depend on Δm^2_{41} because the fast oscillations are averaged by the finite resolution of the detector. The transition probability depends on the three small mixing angles $s_{13}, s_{14}, s_{24} \simeq 0.15$, which can be all assumed to be of the same order ϵ. Another small quantity is the ratio of the solar and atmospheric squared-mass splittings $\alpha \equiv \Delta m^2_{12}/\Delta m^2_{13} \simeq \pm 0.03$, which is of order ϵ^2. Remarkably, for values of the mixing angles indicated by the current global 3-flavor analyses [3–6] (for θ_{13}) and the $3+1$ fits [9–12] (for θ_{14} and θ_{24}), the size of the new (atmospheric-sterile) interference term is basically identical to that of the standard (solar-atmospheric) interference term [2]. This implies that T2K and NOνA are sensitive to both CP-phases δ_{13} and δ_{14}.

Finally, we mention that the matter effects slightly modify the transition probability, leaving unaltered its decomposition in the sum of three contributions. We refer the reader to [1] for a detailed treatment of matter effects in the 3+1 scheme. Here, we just recall that they introduce a dependency on the dimensionless quantity

$$v = \frac{2VE}{\Delta m^2_{31}} \,, \tag{10}$$

where

$$V = \sqrt{2} G_F N_e \tag{11}$$

is the constant matter potential along the neutrino trajectory in the Earth crust. We have $v \simeq 0.05$ in T2K and $v \simeq 0.17$ in NOνA at the energy corresponding to the first oscillation maximum ($E \simeq 0.6$ GeV in T2K, $E \simeq 2$ GeV in NOνA). Therefore, the matter effects are appreciable only in NOνA and confer to this experiment an enhanced sensitivity to the neutrino mass hierarchy.

V. DATA USED AND DETAILS OF THE ANALYSIS

For the determination of the two active-sterile mixing angles θ_{14} and θ_{24} we use the update of the analysis in Ref. [28] presented in Ref. [29]. We considered the data of the following three groups of experiments:

(A) The $\overset{(-)}{\nu}_\mu \to \overset{(-)}{\nu}_e$ appearance data of the LSND [17], MiniBooNE [30, 31], BNL-E776 [32], KARMEN [33], NOMAD [34], ICARUS [35] and OPERA [36] experiments. The two last ones have been treated following the approach described in [37]. We did not consider the anomalous low-energy bins of the MiniBooNE experiment [30, 31], according to the "pragmatic" approach advocated in Ref. [9].

(B) The following $\overset{(-)}{\nu}_e$ disappearance data: 1) the data of the Bugey-4 [38], ROVNO91 [39], Bugey-3 [40], Gosgen [41], ILL [42], Krasnoyarsk [43], Rovno88 [44], SRP [45], Chooz [46], Palo Verde [47], Double Chooz [48], and Daya Bay [49] reactor antineutrino experiments with the new theoretical fluxes [25–27, 50]; 2) the data of the GALLEX [23] and SAGE [24] Gallium radioactive source experiments with the statistical method discussed in Ref. [21], considering the recent ^{71}Ga(^{3}He, ^{3}H)^{71}Ge cross section measurement in Ref. [51]; 3) the solar neutrino constraint on $\sin^2 2\theta_{ee}$ [22, 52–55]; 4) the KARMEN [56] and LSND [57] $\nu_e + {}^{12}{\rm C} \to {}^{12}{\rm N}_{\rm g.s.} + e^-$ scattering data [58], with the method discussed in Ref. [59].

(C) The constraints on $\overset{(-)}{\nu}_\mu$ disappearance obtained from the data of the CDHSW experiment [60], from the analysis [61] of the data of atmospheric neutrino oscillation experiments, from the analysis [62, 63] of the MINOS neutral-current data [64] and from the analysis of the SciBooNE-MiniBooNE data neutrino [65] and antineutrino [66] data. We have not included the IceCube results recently reported in [67]. However, this has no impact in our results, because, as already noted in [29], these data modify the upper bounds on θ_{24} only for values of Δm^2_{41} which are lower then $\sim 1\,{\rm eV}^2$. This conclusion is

corroborated by the numerical analysis performed in [12].

Concerning the LBL experiments, we use the preliminary data released at the Neutrino 2016 and ICHEP 2016 conferences by the NOνA [7] and T2K [8] collaborations, considering the neutrino and antineutrino datasets, and including both the appearance and disappearance channels. In order to calculate the theoretical expectation for the total number of events and their binned spectra in the reconstructed neutrino energy, we use the software GLoBES [68, 69]. As input information we use the unoscillated ν_μ and $\overline{\nu}_\mu$ fluxes extrapolated at the far detector from Ref. [70, 71] for T2K and from Ref. [72] for NOνA. The analysis for the appearance channel is performed using the total rate information as in [1, 2], which presents very small differences with respect to the analysis done using the full energy spectrum. This is due to three factors: i) the off-axis configuration of NOνA and T2K, which leads to a narrow energy spectrum peaked around the first oscillation maximum; ii) the limited statistics currently available in the appearance channel both in NOνA and T2K; iii) the smearing induced by the finite energy resolution of the far detectors. Differently, for the disappearance channel we perform a full spectral analysis of the far detector event distribution, since in this case the energy information has a crucial role.

In the standard 3-flavor case, the free parameters in the analysis are the atmospheric mass splitting Δm^2_{32}, the two mixing angles θ_{13}, θ_{23} and the CP-phase δ_{13}. In the 4-flavor analysis, in addition, we consider as free parameters Δm^2_{41}, θ_{14}, θ_{24} and the CP-phase δ_{14}. We fix $\theta_{34} = 0$, beacause the perturbations induced by non-zero θ_{34} are very small in T2K and NOνA. We have explicitly checked numerically that for non-zero values of θ_{34} currently allowed by data, the oscillation probabilities in both the appearance and disappearance channels are almost indistinguishable from those calculated with $\theta_{34} = 0$. Finally, we mention that both in the 3-flavor and 4-flavor analyses we fix the solar mass-mixing parameters at their best fit values obtained in the global 3-flavor analysis [3].

As pointed out in Ref. [1], in the 4-flavor scenario, the analysis has to deal with the fact that the near detectors in the long-baseline experiments T2K and NOνA are sensitive to the oscillations induced by the extra sterile neutrino. The neutrino fluxes used in the standard analysis are constrained with the information extracted from the near detectors under the assumption of no oscillation at short baselines, which is true only for three flavors. With the addition of an extra neutrino with $\Delta m^2_{41} \sim O(1\ \mathrm{eV}^2)$, the survival probability for ν_μ at the near detector can be approximated as

$$P^{4\nu,\mathrm{ND}}_{\mu\mu} \simeq 1 - 4\sin^2\theta_{24}\sin^2\left(\frac{\Delta m^2_{41} L}{4E}\right) . \qquad (12)$$

Therefore, a suppression of the fluxes that depends on the parameters Δm^2_{41}, θ_{24} and on the the energy is expected. A precision analysis of the LBL data in the 3+1 scheme would require the simultaneous treatment of the near and far detector. However, the spectrum of events expected at the near detector is problematic to reproduce, since many details are not accessible from outside the collaborations. To circumvent this problem we have incorporated the effects of the oscillation at the near detector using the following approximate procedure. We have corrected the expected distribution of events at the far detector multiplying it by the energy dependent factor $1/P^{4\nu,\mathrm{ND}}_{\mu\mu}$, taking its averaged value in each energy bin. In this way, we approximately untie the far detector fluxes from their dependency on the oscillations occurred at the near detector. We have checked that these corrections introduce small modifications on our final results. Hence, our approximate approach is justified. However, we stress that a more detailed analysis in the 3+1 scheme should incorporate the simultaneous fit of the native neutrino fluxes with the near and far detector data for varying values of the parameters Δm^2_{41} and θ_{24}. At the moment, this is possible only from inside the experimental collaborations.

As a separate analysis, we constrain the value of θ_{13} using the far-to-near ratios of the reactor θ_{13}-sensitive experiments Daya-Bay and RENO. Their data are analyzed using the total rate information following the approach described in Ref. [73]. For both experiments we have used the latest data [74, 75] based, respectively, on 1230 live days (Daya Bay) and 500 live days (RENO), recently released at the Neutrino 2016 conference. Since the fast oscillations induced by Δm^2_{14} are averaged out at both near and far detector sites, the far-to-near ratios of Daya Bay and RENO are not sensitive to 4-flavor effects. Therefore, the estimate of θ_{13} is identical in the 3-flavor and 3+1 schemes.

VI. NUMERICAL RESULTS

A. Constraints on the new mixing angles (θ_{14}, θ_{24}) and the new CP-phase δ_{14}

Figure 1 and 2 represent the bidimensional projections of the $\Delta\chi^2$ for normal hierarchy (NH) and inverted hierarchy (IH) in the planes $[\sin^2\theta_{14}, \delta_{14}]$, $[\sin^2\theta_{14}, \sin^2\theta_{24}]$ and $[\delta_{14}, \sin^2\theta_{24}]$ for the top left, bottom left and bottom right panels respectively. The three contours are drawn for $\Delta\chi^2 = 1,\ 2.7,\ 4$, corresponding to 1σ, 90% and 2σ for 1 d.o.f. The allowed regions in the $[\sin^2\theta_{14}, \sin^2\theta_{24}]$ plane are almost the same of those (not shown) that we obtain by the fit of the SBL data taken alone. This finding can be understood by observing that the SBL experiments currently dominate over the LBL ones in the determination of the two new mixing angles. The preferred values of $\sin^2\theta_{14}$ and $\sin^2\theta_{24}$ lie in the range [0.01-0.03], which means that the new mixing angles θ_{14} and θ_{24} are of the same order of magnitude of the standard mixing angle θ_{13} (we recall that $\sin^2\theta_{13} \simeq 0.025$). A quick estimate

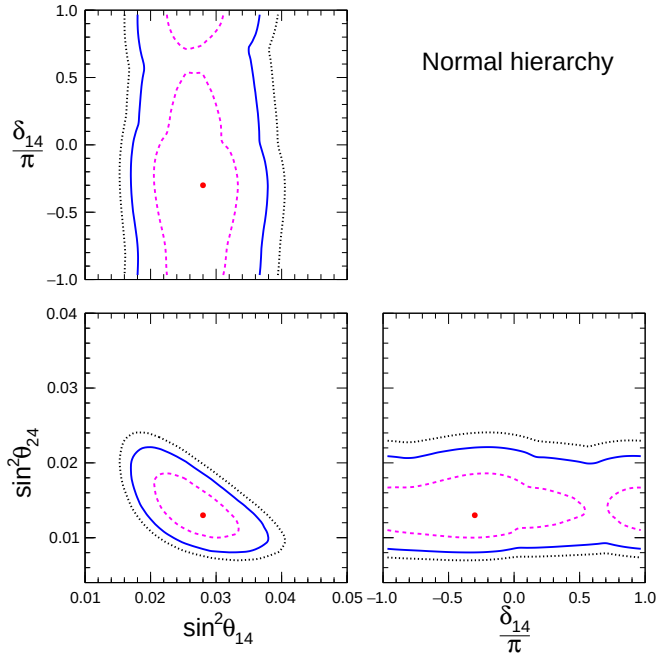

FIG. 1: Regions allowed by the combination of the SBL and LBL data (T2K and NOνA) together with the θ_{13}-sensitive reactor results for the NH case. The left-bottom panel reports the projection on the plane of the two mixing angles $(\theta_{14}, \theta_{24})$. The other two panels display the constraints in the plane formed by each one of these two mixing angles and the new CP-phase δ_{14}. The confidence levels correspond to 1σ, 90% and 2σ for 1 d.o.f ($\Delta\chi^2 = 1,\ 2.7,\ 4$), and the best-fit points are marked with a red point.

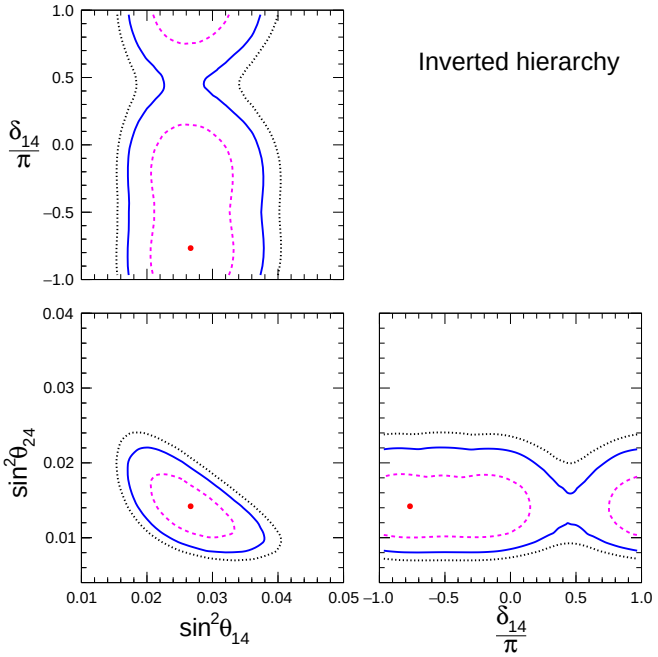

FIG. 2: Regions allowed by the combination of the SBL and LBL data (T2K and NOνA) together with the θ_{13}-sensitive reactor results for the IH case. The left-bottom panel reports the projection on the plane of the two mixing angles $(\theta_{14}, \theta_{24})$. The other two panels display the constraints in the plane formed by each one of these two mixing angles and the new CP-phase δ_{14}. The confidence levels correspond to 1σ, 90% and 2σ for 1 d.o.f ($\Delta\chi^2 = 1,\ 2.7,\ 4$), and the best-fit points are marked with a red point.

of the amplitude of the new interference term in Eq. (9) reveals that its size is similar to that of the standard interference term in Eq. (8). Therefore, it is quite natural to expect that the LBL data will posses some sensitivity to the new CP-phase δ_{14}. This qualitative conclusion is validated by our numerical results displayed in the top left and bottom right panels of Figs. 1 and 2. It is important to observe that the input from the SBL experiments is essential for the extraction of the information on δ_{14} from the LBL setups, since these last ones have a very scarce sensitivity to θ_{14} and θ_{24}, and therefore are unable to constrain the amplitude of the new interference term in Eq. (9). In addition, we underline that also the precise determination of θ_{13} attained independently by the reactor experiments Daya Bay and RENO, plays a relevant role in constraining the new CP-phase δ_{14}, because it helps to constrain the magnitude of the leading term in Eq. (7) (proportional to s^2_{13}) and the amplitude of the two standard interference terms (which are both proportional to s_{13}). A comparison of our results with those presented in [1, 2] shows that the 68% and 90% bounds on δ_{14} are slightly weaker, despite the improved statistics accumulated in the LBL data. This is due to having taken into account the uncertainty on θ_{14} and θ_{24}, which in [1, 2] were both fixed to $\sin^2\theta_{14} = \sin^2\theta_{24} = 0.025$.

B. Correlation between the two CP-phases δ_{13} and δ_{14}

Figure 3 shows the constraints in the plane of the two CP-phases $[\delta_{14}, \delta_{13}]$ for NH (IH) left panel (right panel). Also in this figure, the regions are obtained combining the SBL data, the LBL results from NOνA and T2K, and the data from Daya-Bay and RENO. In both mass hierarchies the CP-conserving cases $\delta_{13} = 0, \pi$ are disfavored at $\Delta\chi^2 \simeq 2.7$. The best fit value $\delta_{13} \simeq -\pi/2$, is basically the same obtained in the 3-flavor case (see the analyses [3–6]). This preference comes from the observation of an excess (deficit) of ν_e ($\bar{\nu}_e$) events with respect to the expectations for the appearance channel $\nu_\mu \to \nu_e$ ($\bar{\nu}_\mu \to \bar{\nu}_e$), when assuming a value of θ_{13} equal to the best fit point of reactor experiments. In fact, Eq. (8) shows that, around the first oscillation maximum ($\Delta = \pi/2$), the standard interference term is proportional to $\sin\delta_{13}$.[2] This implies that this term is maximized (minimized) for neutrinos (antineutrinos) for $\delta_{13} = -\pi/2$ in agreement

[2] We recall that the when passing from neutrino to antineutrino probability one has to invert the sign of all the CP-phases.

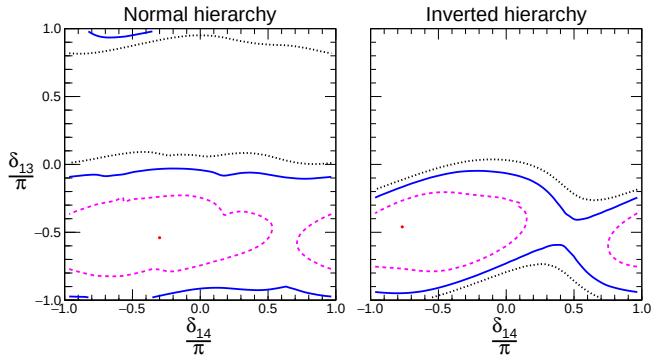

FIG. 3: Regions allowed by the combination of the SBL and LBL data (T2K and NOνA) together with the θ_{13}-sensitive reactor results for NH (left panel) and IH (right panel) in the plane spanned by the two CP phases δ_{13} and δ_{14}. The confidence levels are the same ones used in Fig. 1.

with the observed pattern. Our numerical analysis in the 3+1 scheme reveals that the presence of the new interference terms does not spoil this picture. This behavior can be explained by observing that at the first oscillation maximum ($\Delta = \pi/2$) the new interference term is proportional to $\cos(\delta_{13} - \delta_{14})$, and therefore (in contrast to the standard term) its sign is the same for neutrinos and antineutrinos. We observe that for $\delta_{13} \simeq \delta_{14} \simeq -\pi/2$, the new interference term assumes its maximal positive value (for both neutrinos and antineutrinos). In the fit the neutrino dataset dominates over the (lower statistics) antineutrino data set and, as a consequence, the excess of ν_e's wins over the deficit of $\bar{\nu}_e$'s, driving the new CP-phase to a best fit value close to $\delta_{14} \simeq -\pi/2$.

C. Impact of sterile neutrinos on the standard neutrino properties

In the previous subsections we have focused our discussion on the new parameters of the 3+1 scheme and to the correlation among the two CP-phases. However, it is of interest to see what happens to the estimates of the standard parameters, which were marginalized in the figures shown until now. In particular, it seems of particular interest to assess the robustness/fragility of the estimate of the CP-phase $\delta \equiv \delta_{13}$, the mass hierarchy and the mixing angle θ_{23}, which all are at the center of current investigations.

Figure 4 displays the regions allowed in the plane $[\sin^2 2\theta_{13}, \delta_{13}]$ by the joint analysis of all the SBL experiments and the two LBL experiments T2K and NOνA. The two upper panels correspond to the 3-flavor framework,[3] while the two lower ones are obtained in the 4-flavor scheme. The two left (right) panels refer to NH (IH). The interval of θ_{13} identified by the reactor experiments at 68% C.L. (represented by the green vertical band) is displayed for the sake of comparison. In all cases Δm^2_{32} and the mixing angle θ_{23} are marginalized away. In addition, in the 4-flavor case, we marginalize over the two mixing angles (θ_{14}, θ_{24}) and the CP-phase δ_{14}. The contours represented in the plots correspond to the same confidence levels reported in the previous plots. The comparison of the 3-flavor and 4-flavor allowed regions shows the following features: i) the range allowed by LBL alone for θ_{13} is appreciably larger in the 4-flavor case. This is a consequence of the presence of the new interference term, which allows larger excursions of the transition probability from its average value. However, one can understand that, once the reactor data sensitive to θ_{13} (Daya Bay and RENO) are included in the fit, θ_{13} is "fixed" with high precision in both 3-flavor and 4-flavor schemes; ii) the constraints on the CP-phase δ_{13} are basically identical in the two schemes. In both cases there is a preference (rejection) of values of $\sin\delta_{13} < 0$ ($\sin\delta_{13} > 0$). We have already discussed this point in the description of Fig. 3 concerning the correlation on the two CP-phases; iii) in both schemes the allowed regions, at low confidence levels, present two lobes, which are more pronounced in the 3-flavor case. This feature is imputable to the swap of the best fit value of θ_{23} among the two quasi-degenerate non-maximal solutions, one in the lower octant (LO) and the other one in the higher octant (HO). We will discuss further this point when commenting Fig. 5.

Figure 4 also evidences appreciable differences between the two cases of NH and IH, which can be traced to the presence of the matter effects. As discussed in Sec. IV, the matter potential tends to increase (decrease) the theoretically expected ν_e rate in the case of NH (IH). The opposite is true for $\bar{\nu}_e$'s but their weight in the analysis is lower, so the neutrino data sets dominate. In addition, as discussed in Sec. IV, the NOνA ν_e data are more sensitive than the T2K ν_e data to the matter effects. More specifically, the following differences among the two hierarchies emerge, which are present both in the 3-flavor and 4-flavor schemes. The regions obtained for the case of IH are shifted towards larger values of θ_{13} and are slightly wider in the variable θ_{13} with respect to those obtained in the NH case. In addition, in the IH case, the fit tends to prefer (reject) values of $\sin\delta_{13} < 0$ ($\sin\delta_{13} > 0$) in a more pronounced way.

[3] It should be noted that at the SBL experiments the 3-flavor effects are completely negligible. Consequently, one can adopt two different approaches when considering the 3-flavor scheme: i) include the SBL data in the fit, ii) exclude them from the fit. What changes between the two approaches is only the value of the absolute minimum of the χ^2. Following the first option, one obtains a much higher value than following the second one. This just corresponds to the fact that in the 3+1 scheme the goodness of fit increases, because the sterile oscillations are able to fit the SBL data. However, when one is interested in parameter estimation, only the expansion of the χ^2 around its absolute minimum matters and the choice of including or not including the SBL data in the fit is irrelevant.

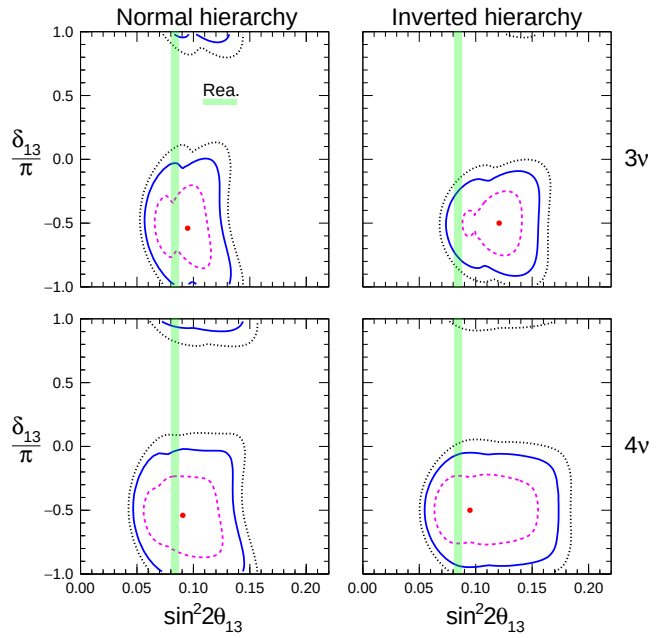

FIG. 4: Regions allowed in the plane $[\sin^2 2\theta_{13},\ \delta_{13}]$ by the joint analysis of all the SBL experiments and the LBL experiments (T2K and NOνA). The interval of θ_{13} identified by the reactor experiments (green vertical band) is displayed for the sake of comparison. The left (right) panels represent the NH (IH) case. The upper (lower) panels refer to the 3-flavor (4-flavor) scheme. The confidence levels are the same reported in Fig. 1.

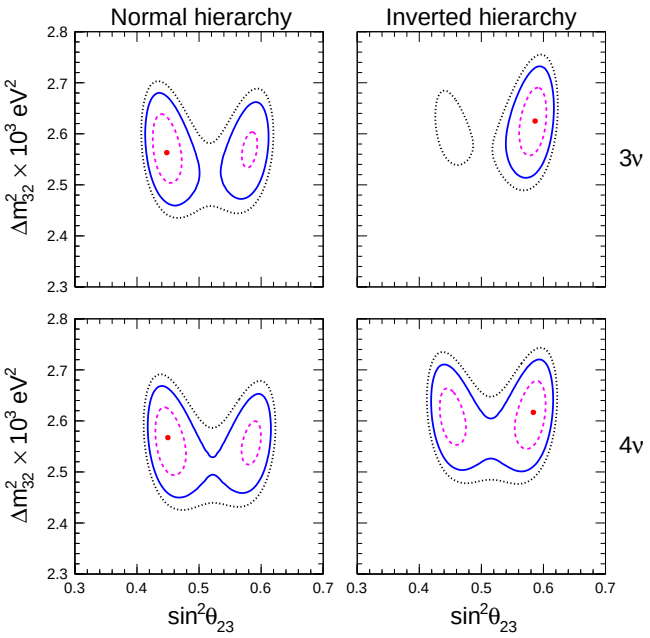

FIG. 5: Regions allowed in the plane $[\sin^2\theta_{23},\ \Delta m^2_{32}]$ by the joint analysis of all the SBL, the LBL data (T2K and NOνA), together with the θ_{13}-sensitive reactor results. The left (right) panels represent the NH (IH) case. The upper (lower) panels refer to the 3-flavor (4-flavor) scheme. The confidence levels are the same reported in Fig. 1.

After marginalizing over all parameters we can calculate the $\Delta\chi^2$(IH-NH) difference between normal and inverted hierarchy

$$\Delta\chi^2(\text{IH-NH}) = \chi^2_{\text{min}}(\text{IH}) - \chi^2_{\text{min}}(\text{NH})\ . \qquad (13)$$

For the 3-flavors (4-flavors) analysis of the LBL data alone we obtain $\Delta\chi^2(\text{IH-NH}) \simeq 1.0$ (0.8). Therefore this data are (still) not sensitive to the mass hierarchy. The situation sensibly changes when the reactor experiments sensitive to θ_{13} are included in the fit. In fact, the combination of LBL and reactor provides a slight preference for NH: $\Delta\chi^2(\text{IH-NH}) \simeq 2.0$ (1.3) in the 3-flavor (4-flavors) case. The reduced value obtained in the 3+1 framework is due to the inevitable widening of the parameter space in the presence of an additional neutrino. The preference for the NH case can be understood comparing the allowed regions from T2K and NOνA with the constraint on $\sin^2 2\theta_{13}$ from reactor experiments (vertical green band in Fig. 4. One notes that there is a better agreement for NH, whereas for IH the separation between the two best fit points is at the level of about $\sim 1\sigma$.

Let us now come to the estimate of the standard mixing angle θ_{23}. Recently, the disappearance analysis of the NOνA collaboration [7] has reported a preference for non-maximal θ_{23} at the level of 2.5σ. The latest 3-flavor global fits [4, 5] have shown that this feature persists at the level of 2σ even when other datasets are included in the analysis. Given the important role of the atmospheric angle θ_{23} in the context of model building, it seems opportune to assess the estimate of such a parameter in the enlarged 3+1 scheme. Figure 5 reports the allowed regions in the plane $[\sin^2\theta_{23}, \Delta m^2_{32}]$, all the other parameters having being marginalized away. The left (right) panels refer to normal (inverted) hierarchy, while the upper (lower) panels refer to the 3-flavor (4-flavor) case. In both schemes we have included in the analysis all the SBL data, the LBL results from T2K and NOνA (both appearance and disappearance channels) and the θ_{13}-sensitive reactor experiments. The results reported in the upper panels confirm the preference for non maximal mixing in the 3-flavor scenario. Maximal mixing is disfavored at about 2σ. We note that there is a change in the best fit octant when switching from normal to inverted hierarchy. This is a consequence of the anticorrelation between θ_{13} and θ_{23}, introduced by the appearance data set: the lower θ_{13} the higher the value of θ_{23}. In IH we find a preference for the higher octant ($\theta_{23} > 45^0$) at almost two standard deviations. The two lower panels depict how the situation changes in the 4-flavor scheme. We can observe that the preference for non maximal mixing survives almost unaltered in both NH and IH. Therefore, it seems that the preference for non maximal θ_{23} is a robust feature, which is independent of the scheme adopted (3-flavor or 4-flavor). In contrast, we see that the preference for $\theta_{23} > 45^0$ found in IH (right upper panel) completely disappears in the 3+1 scheme (right lower panel). This behavior confirms the results of the sensitivity study performed in [76], where it has been

shown that new interference term induced by the sterile neutrino in the $\nu_\mu \to \nu_e$ transition probability can completely wash out the sensitivity to the octant of θ_{23}, even in future experiments like DUNE, which will make use of a high-intensity broad-band neutrino beam. Our analysis performed with the real data confirms such a general behavior, showing that the indication on the octant of θ_{23} becomes a fragile feature in the 3+1 scheme.

VII. CONCLUSIONS

We have shown that, within the 3+1 scheme, the combination of the existing SBL data with the LBL results coming from the two currently running experiments NOνA and T2K, enables us to simultaneously constrain two active-sterile mixing angles θ_{14} and θ_{24} and two CP-phases $\delta_{13} \equiv \delta$ and δ_{14}. The two mixing angles are basically determined by the SBL data, while the two CP-phases are identified by the LBL experiments, once the information coming from the SBL setups is taken into account. We have also assessed the robustness/fragility of the estimates of the standard 3-flavor properties in the more general 3+1 scheme. To this regard we found that: i) the indication of CP-violation found in the 3-flavor analyses persists also in the 3+1 scheme, with $\delta_{13} \equiv \delta$ having still its best fit value around $-\pi/2$; ii) the 3-flavor weak hint in favor of the normal hierarchy becomes even less significant when sterile neutrinos come into play; iii) the indication of non-maximal θ_{23} (driven by NOνA) appears to be robust in the 3+1 scheme; iv) the preference in favor of one of the two octants of θ_{23} found in the 3-flavor framework (higher octant for inverted mass hierarchy) is completely washed out in the 3+1 scheme. We hope that our joint analysis of SBL and LBL data in the 3+1 scheme may serve as a guide for more comprehensive analyses and may increase the awareness of the neutrino community towards the important role of LBL experiments in the search of CP violation induced by light sterile neutrinos.

Acknowledgments

This work was partially supported by the research grant *Theoretical Astroparticle Physics* number 2012CPPYP7 under the program PRIN 2012 funded by the Italian Ministero dell'Istruzione, Università e della Ricerca (MIUR) and by the research project *TAsP* funded by the Instituto Nazionale di Fisica Nucleare (INFN). A. P. is supported by the project *Beyond three neutrino families* within the FutureInResearch program, Fondo di Sviluppo e Coesione 2007-2013, APQ Ricerca Regione Puglia Programma regionale a sostegno della specializzazione intelligente e della sostenibilità sociale ed ambientale.

[1] N. Klop and A. Palazzo, Phys. Rev. **D91**, 073017 (2015), 1412.7524.
[2] A. Palazzo, Phys. Lett. **B757**, 142 (2016), 1509.03148.
[3] F. Capozzi, E. Lisi, A. Marrone, D. Montanino, and A. Palazzo, Nucl. Phys. **B908**, 218 (2016), 1601.07777.
[4] A. Marrone (2016), presented at the 27th International Conference on Neutrino Physics and Astrophysics in July 2016 in London,.
[5] I. Esteban, M. C. Gonzalez-Garcia, M. Maltoni, I. Martinez-Soler, and T. Schwetz (2016), 1611.01514.
[6] D. V. Forero, M. Tortola, and J. W. F. Valle, Phys.Rev. **D90**, 093006 (2014), arXiv:1405.7540.
[7] P. Vahle (2016), presented at the 27th International Conference on Neutrino Physics and Astrophysics in July 2016 in London,.
[8] K. Iwamoto (2016), presented at the 38th International Conference on High Energy Physics in August 2016 in Chicago,.
[9] C. Giunti, M. Laveder, Y. Li, and H. Long, Phys.Rev. **D88**, 073008 (2013), arXiv:1308.5288.
[10] J. Kopp, P. A. N. Machado, M. Maltoni, and T. Schwetz, JHEP **05**, 050 (2013), 1303.3011.
[11] G. H. Collin, C. A. Arguelles, J. M. Conrad, and M. H. Shaevitz, Nucl.Phys. **B908**, 354 (2016), arXiv:1602.00671.
[12] G. H. Collin, C. A. Argelles, J. M. Conrad, and M. H. Shaevitz, Phys. Rev. Lett. **117**, 221801 (2016), 1607.00011.
[13] S. K. Agarwalla, S. S. Chatterjee, A. Dasgupta, and A. Palazzo, JHEP **02**, 111 (2016), 1601.05995.
[14] S. K. Agarwalla, S. S. Chatterjee, and A. Palazzo, JHEP **09**, 016 (2016), 1603.03759.
[15] S. M. Bilenky, C. Giunti, and W. Grimus, Eur. Phys. J. **C1**, 247 (1998), hep-ph/9607372.
[16] C. Athanassopoulos et al. (LSND), Phys. Rev. Lett. **75**, 2650 (1995), nucl-ex/9504002.
[17] A. Aguilar et al. (LSND), Phys. Rev. **D64**, 112007 (2001), hep-ex/0104049.
[18] J. N. Abdurashitov et al. (SAGE), Phys. Rev. **C73**, 045805 (2006), nucl-ex/0512041.
[19] M. Laveder, Nucl. Phys. Proc. Suppl. **168**, 344 (2007).
[20] C. Giunti and M. Laveder, Mod. Phys. Lett. **A22**, 2499 (2007), hep-ph/0610352.
[21] C. Giunti and M. Laveder, Phys. Rev. **C83**, 065504 (2011), arXiv:1006.3244.
[22] C. Giunti, M. Laveder, Y. Li, Q. Liu, and H. Long, Phys. Rev. **D86**, 113014 (2012), arXiv:1210.5715.
[23] F. Kaether, W. Hampel, G. Heusser, J. Kiko, and T. Kirsten, Phys. Lett. **B685**, 47 (2010), arXiv:1001.2731.
[24] J. N. Abdurashitov et al. (SAGE), Phys. Rev. **C80**, 015807 (2009), arXiv:0901.2200.
[25] G. Mention et al., Phys. Rev. **D83**, 073006 (2011), arXiv:1101.2755.
[26] T. A. Mueller et al., Phys. Rev. **C83**, 054615 (2011), arXiv:1101.2663.
[27] P. Huber, Phys. Rev. **C84**, 024617 (2011), arXiv:1106.0687.

[28] S. Gariazzo, C. Giunti, M. Laveder, Y. Li, and E. Zavanin, J. Phys. **G43**, 033001 (2016), arXiv:1507.08204.

[29] C. Giunti (2016), Proceedings of the 27th International Conference on Neutrino Physics and Astrophysics (Neutrino 2016) London, United Kingdom, July 4-9, 2016, 1609.04688.

[30] A. A. Aguilar-Arevalo et al. (MiniBooNE), Phys. Rev. Lett. **102**, 101802 (2009), arXiv:0812.2243.

[31] A. Aguilar-Arevalo et al. (MiniBooNE), Phys.Rev.Lett. **110**, 161801 (2013), arXiv:1303.2588.

[32] L. Borodovsky et al. (BNL-E776), Phys. Rev. Lett. **68**, 274 (1992).

[33] B. Armbruster et al. (KARMEN), Phys. Rev. **D65**, 112001 (2002), hep-ex/0203021.

[34] P. Astier et al. (NOMAD), Phys. Lett. **B570**, 19 (2003), hep-ex/0306037.

[35] M. Antonello et al. (ICARUS), Eur.Phys.J. **C73**, 2599 (2013), arXiv:1307.4699.

[36] N. Agafonova et al. (OPERA), JHEP **1307**, 004 (2013), arXiv:1303.3953.

[37] A. Palazzo, Phys.Rev. **D91**, 091301 (2015), arXiv:1503.03966.

[38] Y. Declais et al. (Bugey), Phys. Lett. **B338**, 383 (1994).

[39] A. Kuvshinnikov, L. Mikaelyan, S. Nikolaev, M. Skorokhvatov, and A. Etenko, JETP Lett. **54**, 253 (1991).

[40] B. Achkar et al. (Bugey), Nucl. Phys. **B434**, 503 (1995).

[41] G. Zacek et al. (CalTech-SIN-TUM), Phys. Rev. **D34**, 2621 (1986).

[42] A. Hoummada, S. Lazrak Mikou, G. Bagieu, J. Cavaignac, and D. Holm Koang, Applied Radiation and Isotopes **46**, 449 (1995).

[43] G. S. Vidyakin et al. (Krasnoyarsk), Sov. Phys. JETP **71**, 424 (1990).

[44] A. I. Afonin et al., Sov. Phys. JETP **67**, 213 (1988).

[45] Z. D. Greenwood et al., Phys. Rev. **D53**, 6054 (1996).

[46] M. Apollonio et al. (CHOOZ), Eur. Phys. J. **C27**, 331 (2003), hep-ex/0301017.

[47] F. Boehm et al. (Palo Verde), Phys. Rev. **D64**, 112001 (2001), hep-ex/0107009.

[48] Y. Abe et al. (Double Chooz), JHEP **1410**, 86 (2014), arXiv:1406.7763.

[49] F. P. An et al. (Daya Bay), Phys. Rev. Lett. **116**, 061801 (2016), arXiv:1508.04233.

[50] K. N. Abazajian et al. (2012), arXiv:1204.5379.

[51] D. Frekers, H. Ejiri, H. Akimune, T. Adachi, B. Bilgier, et al., Phys. Lett. **B706**, 134 (2011).

[52] C. Giunti and Y. Li, Phys.Rev. **D80**, 113007 (2009), arXiv:0910.5856.

[53] A. Palazzo, Phys. Rev. **D83**, 113013 (2011), arXiv:1105.1705.

[54] A. Palazzo, Phys. Rev. **D85**, 077301 (2012), arXiv:1201.4280.

[55] A. Palazzo, Mod.Phys.Lett. **A28**, 1330004 (2013), arXiv:1302.1102.

[56] B. Armbruster et al. (KARMEN), Phys. Rev. **C57**, 3414 (1998), hep-ex/9801007.

[57] L. B. Auerbach et al. (LSND), Phys. Rev. **C64**, 065501 (2001), hep-ex/0105068.

[58] J. Conrad and M. Shaevitz, Phys. Rev. **D85**, 013017 (2012), arXiv:1106.5552.

[59] C. Giunti and M. Laveder, Phys. Lett. **B706**, 200 (2011), arXiv:1111.1069.

[60] F. Dydak et al. (CDHSW), Phys. Lett. **B134**, 281 (1984).

[61] M. Maltoni and T. Schwetz, Phys. Rev. **D76**, 093005 (2007), arXiv:0705.0107.

[62] D. Hernandez and A. Y. Smirnov, Phys. Lett. **B706**, 360 (2012), arXiv:1105.5946.

[63] C. Giunti and M. Laveder, Phys.Rev. **D84**, 093006 (2011), arXiv:1109.4033.

[64] P. Adamson et al. (MINOS), Phys. Rev. Lett. **107**, 011802 (2011), arXiv:1104.3922.

[65] K. B. M. Mahn et al. (SciBooNE-MiniBooNE), Phys. Rev. **D85**, 032007 (2012), arXiv:1106.5685.

[66] G. Cheng et al. (SciBooNE-MiniBooNE), Phys. Rev. **D86**, 052009 (2012), arXiv:1208.0322.

[67] M. G. Aartsen et al. (IceCube), Phys. Rev. Lett. **117**, 071801 (2016), 1605.01990.

[68] P. Huber, M. Lindner, and W. Winter, Comput. Phys. Commun. **167**, 195 (2005), hep-ph/0407333.

[69] P. Huber, J. Kopp, M. Lindner, M. Rolinec, and W. Winter, Comput. Phys. Commun. **177**, 432 (2007), hep-ph/0701187.

[70] K. Abe et al. (T2K), Phys. Rev. **D87**, 012001 (2013), [Addendum: Phys. Rev.D87,no.1,019902(2013)], 1211.0469.

[71] M. Ravonel Salzgeber (T2K) (2015), 1508.06153.

[72] D. R. Rocco, Ph.D. thesis, Minnesota U. (2016), URL `http://lss.fnal.gov/archive/thesis/2000/fermilab-thesis-2016-15.pdf`.

[73] A. Palazzo, JHEP **10**, 172 (2013), 1308.5880.

[74] Z. Yu (2016), presented at the 27th International Conference on Neutrino Physics and Astrophysics in July 2016 in London,.

[75] K. K. Joo (2016), presented at the 27th International Conference on Neutrino Physics and Astrophysics in July 2016 in London,.

[76] S. K. Agarwalla, S. S. Chatterjee, and A. Palazzo (2016), 1605.04299.